THE X-RAY AFTERGLOWS OF GRB 020813 AND GRB 021004 WITH *CHANDRA* HETGS: POSSIBLE EVIDENCE FOR A SUPERNOVA PRIOR TO GRB 020813

NATHANIEL R. BUTLER,[1] HERMAN L. MARSHALL,[1] GEORGE R. RICKER,[1] ROLAND K. VANDERSPEK,[1] PETER G. FORD,[1] GEOFFREY B. CREW,[1] DONALD Q. LAMB,[2] AND J. GARRETT JERNIGAN[3]

ABSTRACT

We report on the detection of an emission line near 1.3 keV, which we associate with blueshifted hydrogen-like sulfur (S XVI), in a 76.8 ks *Chandra* HETGS spectrum of the afterglow of GRB 020813. The line is detected at 3.3 σ significance. We also find marginal evidence for a line possibly due to hydrogen-like silicon (Si XIV) with the same blueshift. A line from Fe is not detected, although a very low significance Ni feature may be present. A thermal model fits the data adequately, but a reflection model may provide a better fit. There is marginal evidence that the equivalent width of the S XVI line decreases as the burst fades. We infer from these results that a supernova likely occurred $\gtrsim 2$ months prior to the γ-ray burst. We find no discrete or variable spectral features in the *Chandra* HETGS spectrum of the GRB 021004 afterglow.

Subject headings: gamma rays: bursts — supernovae: general — X-rays: general

1. INTRODUCTION

Much evidence has accumulated in recent years connecting long-duration γ-ray bursts (GRBs) (Kouveliotou et al. 1993) to supernovae (SNe). The detection of SN 1998bw in association with GRB 980425 (Galama et al. 1998) and the detection of late-time SN "bumps" in several afterglow light curves (Bloom et al. 1999; Reichart 2001 and references therein), the observed positional coincidences between star-forming regions and long-duration GRB afterglows (e.g. Sahu et al. 1997; Kulkarni et al. 1998, 1999), and the evidence for dust extinction in some GRB afterglows all point toward this association. In this context, X-ray spectroscopic observations of early GRB afterglows are tremendously interesting, because they potentially allow us to view directly the effects of the GRB on the progenitor stellar material and possibly on metals freshly synthesized in the SN.

Several authors have claimed detection of Fe lines in GRB X-ray afterglows (Piro et al. 1999, 2000; Antonelli et al. 2002). Beyond very weak evidence in Piro et al. (2000) for an emission line from H-like S in GRB 991216, Reeves et al. (2002, hereafter R02) are the first to strongly assert evidence for emission from low-Z, multiple-α elements in a GRB X-ray afterglow. If valid, this claim has broad implications for GRB emission models, and it would strongly link GRBs to SNe. The reduction of these data and the statistical significance of the results have been called into question by Borozdin & Trudoyubov (2003) and Rutledge & Sako (2002), respectively. In a follow-up paper (Reeves et al. 2003), the *XMM-Newton* (Jansen et al. 2001) observers address those concerns. Physical interpretations aside, the R02 results are controversial largely because of the small number of observed counts and the low spectral resolution

of the EPIC-pn instrument, which would blur some fraction of the line emission into the continuum. These hinder an accurate measurement of the continuum emission and make it difficult to gauge the significance of discrete spectral features.

We find possible evidence for Si and S emission in the *Chandra X-Ray Observatory* (Weisskopf et al. 2002) High Energy Transmission Grating Spectrometer (HETGS) spectrum of the GRB 020813 afterglow. We detect a Ni K line at very low significance, and we find a strikingly low upper limit to the Fe K line equivalent width. The emitting material is blueshifted with velocity $\sim 0.1c$ relative to the GRB host galaxy. These results add weight to the detections claimed by R02 and Watson et al. (2002). With the HETGS's high spectral resolution, we are able to resolve the line widths, and we are able to accurately separate the line and continuum emission. Because the lines we associate with S and Si are detected in the full data set, we have ~ 5 times more counts to work with than R02, where the line emission is observed during only a short period of time. Moreover, the continuum is an order of magnitude stronger than that reported by R02, possibly indicating, in the case of thermal emission, that a power-law component is also present. This may alternatively be a sign that the lines are produced under reflection.

2. OBSERVATIONS

Using Director's Discretionary Time, two afterglows of GRBs detected and localized by the *High-Energy Transient Explorer* (*HETE*) satellite (Ricker et al. 2003) were observed with the *Chandra* HETGS, approximately 1 day after each burst, and lasting for approximately 1 day. Both bursts were long-duration GRBs, with γ-ray durations of $\gtrsim 100$ s. The γ-ray peak flux from GRB 020813 (Villasenor et al. 2002) was quite high ($\sim 10^{-5}$ ergs cm^{-2} s^{-1}), while the peak flux from GRB 021004 (Shirasaki et al. 2002) was approximately 2 orders of magnitude lower.

Chandra began observing the GRB 020813 afterglow with the HETGS on August 13.990 ($t_{\mathrm{burst}} + 21.02$ hr) and continued until August 14.892 ($t_{\mathrm{burst}} + 42.67$ hr), with a total live

[1] Center for Space Research, Massachusetts Institute of Technology, Cambridge, MA 02139; nrbutler@space.mit.edu, hermanm@space.mit.edu, grr@space.mit.edu, roland@space.mit.edu, pgf@space.mit.edu, gbc@space.mit.edu.

[2] Department of Astronomy and Astrophysics, University of Chicago, Chicago, IL 60637; lamb@pion.uchicago.edu.

[3] Space Sciences Laboratory, University of California, Berkeley, CA 94720; jgj@ssl.berkeley.edu.

time of 76.8 ks. The mean count rate from the HEG and an MEG gratings and the zeroth-order image was 0.12 counts s^{-1} (0.06 counts s^{-1} for the gratings alone). The afterglow candidate reported by Fox & Blake (2002) was detected and was observed to fade in brightness with time according to a power law of index $\alpha = -1.38 \pm 0.06$ ($\chi_\nu^2 = 36.4/24$), consistent with the value reported by Vanderspek et al. (2002) and with measured values in the optical (Malesani et al. 2002). Between 0.6 and 6 keV, we measure a time-averaged flux of 2.2×10^{-12} ergs cm^{-2} s^{-1}.

As first reported by Sako & Harrison (2002), *Chandra* began observing the afterglow of GRB 021004 on October 5.358 ($t_{burst} + 20.49$ hr) and continued until October 6.400 ($t_{burst} + 45.50$ hr), with a total live time of 86.7 ks. The mean count rate from the HEG and MEG gratings and the zeroth-order image was 0.04 counts s^{-1} (0.02 counts s^{-1} in the gratings alone). The afterglow candidate reported by Fox (2002) was detected and was observed to fade in brightness with time. The X-ray light curve appears variable. (Similar variability has been reported in the optical for this afterglow; see, e.g., Halpern et al. 2002.) The temporal fade in flux can be described by a power law with index $\alpha = -0.9 \pm 0.1$ ($\chi_\nu^2 = 83.8/27$), consistent with the values reported by Sako & Harrison (2002) and Holland et al. (2003). The time-averaged flux between 0.6 and 6 keV is measured to be 6.3×10^{-13} ergs cm^{-2} s^{-1}.

The total number of counts detected by *Chandra* in the case of GRB 020813 (GRB 021004) is 6.5 times (2 times) the number of counts detected for GRB 991216 (Piro et al. 2000). We perform a parallel spectral/temporal analysis below for the X-ray afterglow spectra of GRB 020813 and GRB 021004.

3. SPECTRAL FITTING

We reduce the HETGS spectral data from the standard L2 event lists using IDL and custom scripts, described in Marshall et al. (2002). For the zeroth-order spectral data, we use the CIAO[4] processing exclusively. Each data set is corrected for quantum efficiency degradation[5] due to contamination in the ACIS chips, prior to spectral fitting. We also destreak the S4 chip.[6] Spectral fitting and analysis is performed with ISIS.[7] For each observation, we fit the HETGS HEG and HETGS MEG first-order data for the entire observation jointly. The +1 and −1 orders are combined for each grating. The data are then binned to a S/N ≥ 5 per bin, with the bin width restricted to $\delta E/E \leq 0.1$. We define S/N as the background-subtracted number of counts divided by the square root of the sum of the signal counts and the variance in the background. Bins of the maximal width with S/N < 3 are rejected, because of lack of signal. For GRB 020813, this selects an HEG energy range of 0.8–7.6 keV and MEG energy range of 0.6–5.2 keV. For GRB 021004, this selects an HEG energy range of 1.0–4.6 keV and MEG energy range of 0.6–4.7 keV. We fit each model by minimizing χ^2. Unless otherwise noted, all quoted errors are 90% confidence.

3.1. *GRB 020813*

As reported by Vanderspek et al. (2002), we find that an absorbed power-law fit to the first-order spectra requires no absorption column in excess of Galactic value. Therefore, in each model that we consider, we include absorption with N_H frozen to 7.5×10^{20} cm^{-2}.

The data are moderately well fitted by a power law (Fig. 1; $\chi_\nu^2 = 176.0/154$), with photon index $\Gamma = 1.85 \pm 0.04$ and normalization $(5.5 \pm 0.2) \times 10^{-4}$ photons keV^{-1} cm^{-2} s^{-1} at 1 keV. A thermal bremsstrahlung fit is a much poorer fit to the data ($\chi_\nu^2 = 196.7/154$, rejectable at 99% confidence), with $kT = 4.6 \pm 0.5$ keV. We find consistent fits using the zeroth-order data. Of note, a large fraction of the contribution to χ^2 in the case of the HETGS power-law fit arises between 1.2 and 1.5 keV. The addition of a Gaussian component in this energy range improves the χ^2 ($\chi_\nu^2 = 160.5/151$). This improvement is at the 99.9% confidence level according the likelihood ratio test ($\Delta\chi^2 = 15.5$ for 3 additional degrees of freedom). However, this method for determining significance is deprecated (see Protassov et al. 2002), and we present Monte Carlo calculations for the significance below. The line energy is 1.31 ± 0.01 keV, with a width of 8 ± 4 eV (1 σ). The rest-frame equivalent width is 67 ± 32 eV, and the flux is $(1.6 \pm 0.8) \times 10^{-14}$ ergs cm^{-2} s^{-1}. Given the optically measured GRB host-galaxy absorption redshift $z \geq 1.254$ (Price et al. 2002), a likely association for this line is S XVI Kα, blueshifted by $0.12c$ from $z = 1.254$. The χ^2 is marginally improved ($\chi_\nu^2 = 155.7/150$) with the inclusion of an additional Gaussian component of the same width, constrained to lie at predicted energy of Si XIV Kα (1.01 keV at $z = 0.99 \pm 0.01$). From the likelihood ratio test, the confidence for the pair can be estimated as 99.96% ($\Delta\chi^2 = 20.3$ for 4 additional degrees of freedom). Allowing the widths to vary jointly, the best-fit width value is 10 ± 9 eV.

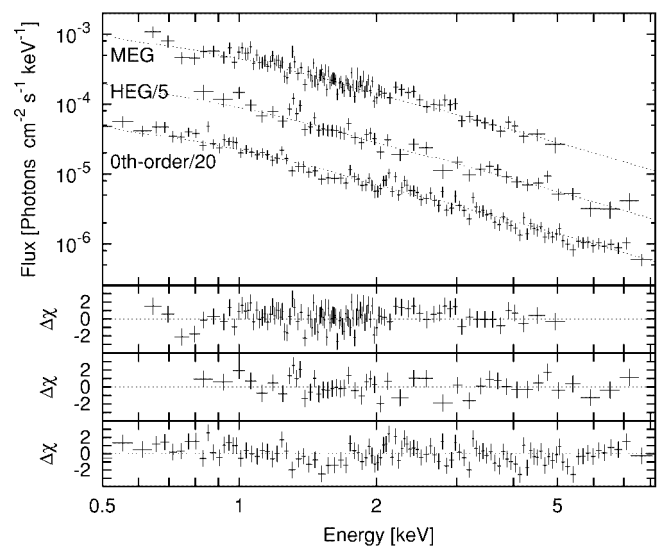In gauging the significance of these features, we must take into account the number of trials performed (i.e., line widths

FIG. 1.—The ±1 order HETGS (HEG/MEG) data for GRB 020813 are moderately well fitted by an absorbed power law (§ 3). The zeroth-order data (S/N ≥ 5 per bin) are also fitted well by this model. Here we divide the HEG data by a factor of 5 and the zeroth-order data by a factor of 20 for ease of viewing.
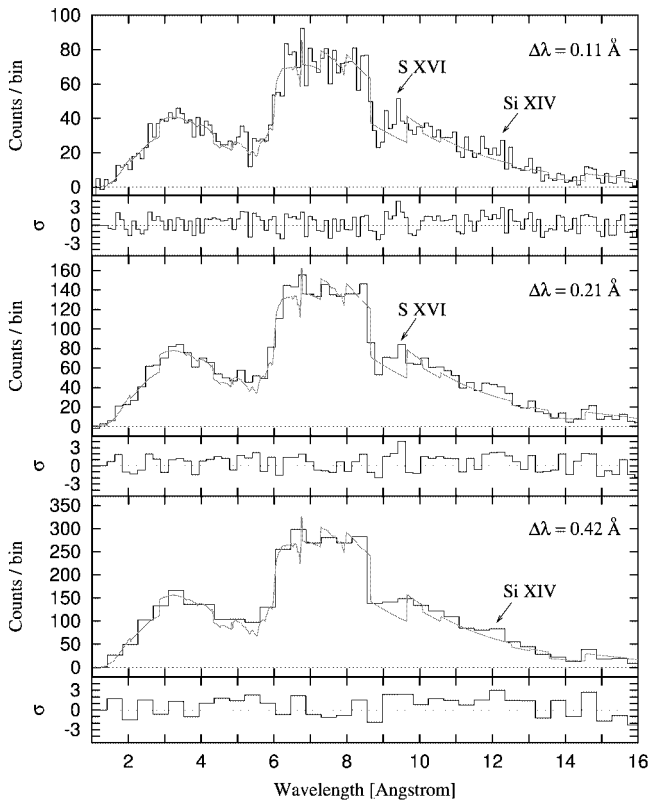
---

[4] See http://cxc.harvard.edu/ciao.
[5] See http://asc.harvard.edu/cal/Acis/Cal_prods/qeDeg.
[6] See http://asc.harvard.edu/ciao/threads/spectra_hetgacis.
[7] See http://space.mit.edu/CXC/ISIS.

FIG. 2.—Best-fit power-law model on top of the combined HETGS HEG+MEG data, at three binnings, for GRB 020813. The significance (reported in σ units) of deviations from the model are calculated using Poisson statistics. We associate the residuals near 9.4 Å in the top and middle plots with H-like S. We associate the high bin near 12.1 Å in the top and bottom plot with H-like Si.

constrained as in the preceding paragraph. No additional features at or above 2.9 σ are present in the HETGS spectrum at the binnings searched. Finally, we derive a 3 σ upper limit of 20 eV for the equivalent widths of any lines unresolved in this search (FWHM $\ll 0.11$ Å) between 6 and 16 Å. This figure grows $\propto \lambda^{-3}$ shortward of 6 Å.

We also attempt to fit these data using a collisional ionization equilibrium (CIE) plasma model, as has been done previously in the case of several recent GRB afterglows observed with *XMM-Newton* (R02; Watson et al. 2002). We form the model using the Astrophysical Plasma Emission Database (APED) accessible through ISIS, with the redshift fixed at $z = 0.99$. We utilize a turbulence velocity v_T, fixed at 2000 km s^{-1}, and thermal line profiles to produce the best-fit line widths above. We fix the abundance of metals lighter than Mg to solar. We tie the Si abundance to the S abundance and allow Ni to vary freely. All other metals are frozen to zero abundance. The CIE plasma fit (Fig. 3; $\chi_\nu^2 = 177.8/152$) is slightly poorer than the pure power-law fit. Allowing the APED metal abundances previously set to zero to vary does not improve the fit. The best-fit plasma temperature is 9.2 ± 1.2 keV. The best-fit S, Si abundance is 2.9 times solar, and the linked abundance is greater than solar at 98% confidence ($\Delta \chi^2 = 5.5$ for 1 additional parameter). The best-fit Ni abundance is 1.8 times solar. There is a low (1.6 σ) significance detection of a Ni K line in the MEG

and line energies searched). Figure 2 displays the power-law model found above overplotted on the summed HEG+ MEG counts, at three binnings. The finest binning is chosen so that each bin between 1.5 and 16.0 Å contains one or more counts. We rebin twice by a factor of approximately 2 in order to look for broader features. The 1.31 keV (9.4 Å) feature is seen in both the top and middle plots at 4.0 σ. This significance describes the Poisson probability that the signal plus background counts could reach a value greater than or equal to the observed values, with the Poisson mean fixed to the number of counts predicted by the model plus the background. The probability for a chance fluctuation of this or greater significance in one or more of the 235 bins shown in Figure 2 is approximately 1.5%, calculated as $P_N \approx 1 - (1 - P_1)^N$. From Monte Carlo simulations of 10^4 spectra using the best-fit power-law model above, we find $P_N = 1.4\%$. From the simulations, we find that the probability for getting two or more 4 σ fluctuations (as observed) is 0.1%. Thus the line is detected at 3.3 σ significance. A broad feature corresponding to the 1.01 keV line mentioned above is observed in the third panel (and also in the first panel) of Figure 2 at ~12.2 Å, with a significance of 2.9 σ. We estimate a 58% probability that a 2.9 σ or greater fluctuation would occur by chance in one or more of the trials. From the Monte Carlo simulations, the probability for getting two or more 2.9 σ fluctuations is 23%. Thus the line is detected at very low (1.2 σ) significance in a blind search, and it is potentially meaningful only if the line location is
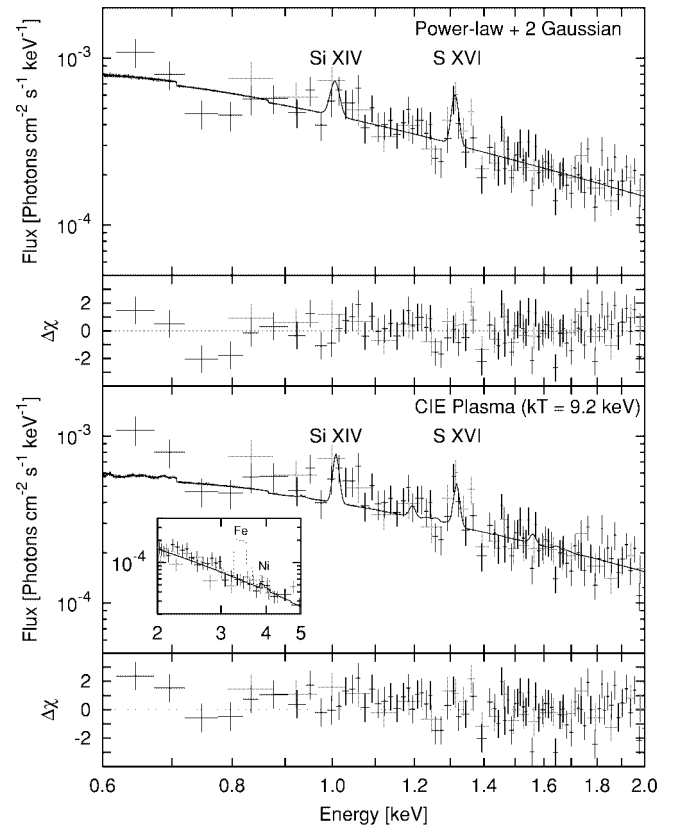

FIG. 3.—Power-law fit to the GRB 020813 ± 1 order HETGS data is improved by adding two Gaussians at the energies of blueshifted (by 0.12c) S XVI Kα and Si XIV Kα. The lines and continuum can be modeled less effectively by a CIE plasma model (*bottom plot*) containing Si, S, and Ni. The inset in the bottom plot shows the 2–5 keV portion of the CIE plasma model fit with (*dotted line*) and without (1.8 times solar abundance in) Fe; an abundance of Fe similar to the abundances for Si and S is strongly ruled out. The HEG data are plotted in gray. The MEG data are plotted in black.

TABLE 1
LINE EMISSION UPPER LIMITS

Element	Abundance	Flux	EW (eV)
Mg....................	4.4	0.5	13
Si......................	5.8	1.9	53
	$(2.9^{+2.9}_{-1.6})$	(1.1 ± 0.8)	(30 ± 23)
S.......................	4.3	2.3	72
	$(2.9^{+1.4}_{-2.0})$	(1.6 ± 0.7)	(50 ± 22)
Ar.....................	1.0	0.2	9
Ca.....................	1.8	0.4	15
Fe.....................	0.1	1.5	100
Ni.....................	4.4	1.5	110
	$(1.8^{+2.6}_{-1.8})$	$1.0^{+0.5}_{-1.0}$	73^{+37}_{-73}

NOTE.—GRB 020813 line emission upper limits at 90% confidence for APED model elemental abundances, H-like Kα line fluxes ($\times 10^{-14}$ ergs cm^{-2} s^{-1}), and rest-frame H-like Kα line equivalent widths. Values are determined from power law plus Gaussian fits. The observer-frame line widths were set via $dE/E = v_t/c \approx 0.0067$. Line centers are set with $z = 0.99$.

spectrum. This features appears as two bins modestly over the power-law fit in Figures 1 and 3 near 4 keV. The APED model fits these bins with a blend of K lines from H and He-like Ni. The APED model with an abundance of Fe comparable to the Si and S abundances would produce a very strong and easily detectable Fe K feature (Fig. 3, *inset*). In Table 1 we report one-parameter 90% confidence upper limits to the abundances of several elements, with upper limits to the line fluxes and rest-frame equivalent widths of H-like K lines in each species. In Figures 4, 5, and 6 we compare the abundances, line luminosities, and rest-frame equivalent widths, respectively, with those reported for other GRB X-ray afterglows.

Since the abundances of α-particle nuclei produced by core-collapse SNe are expected to be approximately the same (see, e.g., Rauscher et al. 2002), relative to solar, the
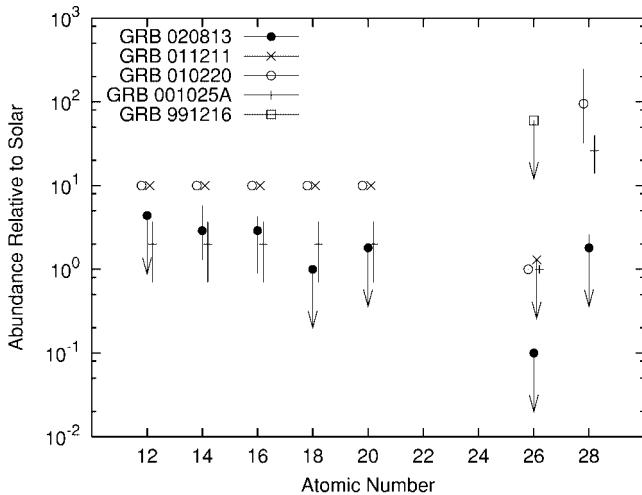

FIG. 5.—Isotropic equivalent line luminosities from Gaussian fits (Table 1) for GRB 020813 (*solid circles*, host at $z = 1.254$) and for several other GRBs in the literature. To determine luminosity distances, we use a cosmology with $\Omega_m = 0.3$, $\Omega_\Lambda = 0.7$, and $h = 0.65$. The values for GRB 011211 come from R02, with $z = 2.14$. The value for GRB 000214 comes from Antonelli et al. (2002), with $z = 0.47$. The value for GRB 991216 has been taken from Piro et al. (2000), using $z = 1$. The value for GRB 970828 comes from Yoshida et al. (1999), using $z = 0.33$. The value for GRB 970508 comes from Piro et al. (1999), using $z = 0.835$. Error bars have been plotted where available.

low relative upper limits that we find for the abundances of Ar and Ca possibly indicate that the Si and S lines are not the result of thermal emission from a hot plasma. After radioactive decay, we would expect an Fe abundance similar to the low-Z, multiple-α metal abundances. This implies that the line fluxes from one or more of the Fe group elements (Fe, Ni, Co) should be higher than we observe. We discuss below the possibility that the lines are due to reflection. An alternative possibility, suggested in part by the APED model's apparent tendency to underfit the

FIG. 4.—Metal abundances for the APED plasma model for GRB 020813 (*filled circles*), as in Table 1. Also plotted are the abundances reported in the literature for several other GRB X-ray afterglow spectra. The values for GRB 011211 come from R02. The values for GRB 010220 and GRB 001025A come from Watson et al. (2002). The value for GRB 991216 has been taken from Piro et al. (2000). Error bars have been plotted where available.
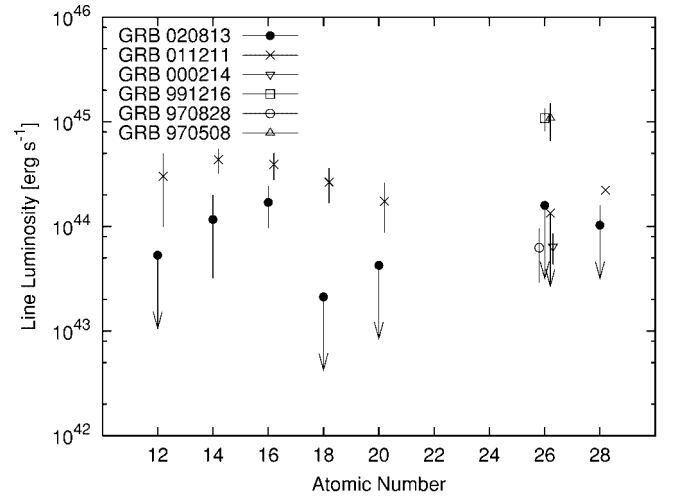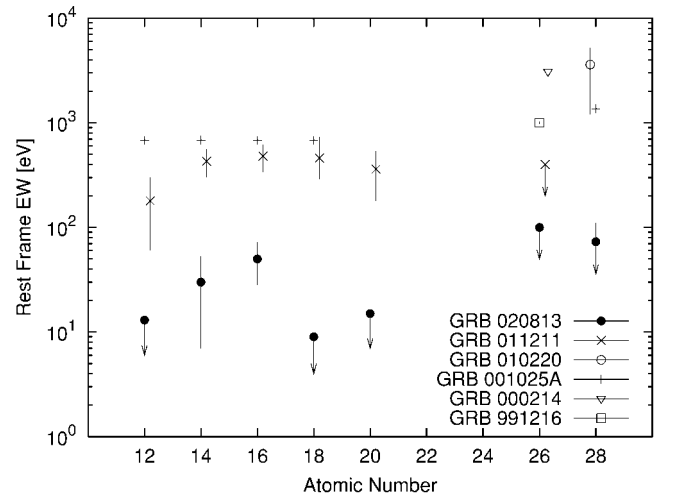

FIG. 6.—Rest-frame equivalent widths in eV from Gaussian fits (Table 1) for GRB 020813 (*filled circles*, $z = 0.99$) and for several other GRBs in the literature. The values for GRB 011211 come from R02, with $z = 1.88$. The values for GRB 010220 ($z = 1.0$) and GRB 001025A ($z = 0.7$) come from Watson et al. (2002). The value for GRB 000214 comes from Antonelli et al. (2002), with $z = 0.47$. The value for GRB 991216 has been taken from Piro et al. (2000), using $z = 1$. Error bars have been plotted where available.

continuum below ~1.5 keV (Fig. 1), is that we must also include a power-law component. It is then possible to use the APED model with a lower temperature (~2 keV), and this weakens the high-energy continuum and the lines from Ar, Ca, and the Fe group elements relative to the Si and S lines. We find models with a single abundance for the α-particle nuclei and Fe that improve upon the power-law fit but do not appear to be as good as the power law plus two-Gaussian fit. Finally, we note that the abundances quoted in Table 1 lose meaning if a power-law component is also present.

3.2. GRB 021004

An absorbed power-law fit to the first-order spectra does not require an absorption column in excess of the Galactic value, as reported by Sako & Harrison (2002). Therefore, in each model that we consider, we include absorption with N_H frozen to 4.24×10^{20} cm^{-2}.

The data are very well fitted by a power law (Fig. 7; $\chi_\nu^2 = 39.5/55$, with $\Gamma = 2.01 \pm 0.08$ and normalization $(1.7 \pm 0.1) \times 10^{-4}$ photons^{-1} keV^{-1} cm^{-2} s^{-1} at 1 keV, consistent with the values found by Sako & Harrison (2002) and Holland et al. (2003). A thermal bremsstrahlung fit is a somewhat poorer, although still very acceptable, fit ($\chi_\nu^2 = 47.2/55$), with $kT = 3.2 \pm 0.4$ keV. We find consistent fits using the zeroth-order data.

We plot the combined HEG/MEG data in count space with the power-law model overplotted in Figure 8 for the same binnings as in Figure 2. No significant features are observed. The largest fluctuation occurs in the middle panel, where one of the ~70 bins reaches 2.6 σ. There is approximately an 89% chance that this would happen by chance in one or more of the bins in that plot. At the 3 σ level, this search is sensitive to moderately broad (FWHM ~ $\delta\lambda$) emission and absorption lines between 6 and 16 Å with equivalent widths greater than 50 eV. Over this same wavelength interval, we derive a 3 σ upper limit of 35 eV to the

FIG. 8.—Best-fit power-law model on top of the combined HETGS HEG+MEG data, at three binnings, for GRB 021004. No highly significant deviations from the model are observed.

equivalent widths of any narrow lines (FWHM $\ll 0.11$ Å). These figures grow $\propto \lambda^{-3}$ shortward of 6 Å. Considering the GRB redshift of 2.328 determined in the optical by Mirabel et al. (2002), several K lines from S, Ar, Ca, Fe, Co, and Ni would have been detected were their equivalent widths larger than these estimated limits.

4. TEMPORAL ANALYSIS

As displayed in Figure 9, the afterglow continua, although moderately variable in the case of GRB 021004, do not appear to evolve spectrally. To search for time-variable discrete features, we divide the summed HEG+ MEG data sets into 2, 4, or 8 portions of equal numbers of counts. For each time section, we examine the counts data at three binnings: 0.11, 0.21, and 0.42 Å (as in Figs. 2 and 8). For each GRB afterglow, we fit absorbed power laws to each of these 42 data sets by minimizing the Cash statistic (Cash 1979). We then search the bins between 1 and 16 Å for deviations from the best-fit model, interpreting the deviations using Poisson statistics as in § 3. We set a limiting detection threshold of 3.7 σ so that fewer than one chance detection is expected in 15 × 235 bins searched. The search yields no emission- or absorption-line detections in the case of GRB 021004, while for GRB 020813 only the Si and S lines (§ 3) are detected. The Si XIV Kα line is detected at 3.7 σ ($P_N \approx 53\%$) in the second quarter (12–28.5 ks) of data, while the S XVI Kα line (three detections) peaks at 4.3 σ ($P_N \approx 6\%$) in the first quarter (12 ks) of data. In Figure 10 we plot the S XVI Kα line flux (measured with Gaussian fits of fixed width and location) and the continuum flux versus
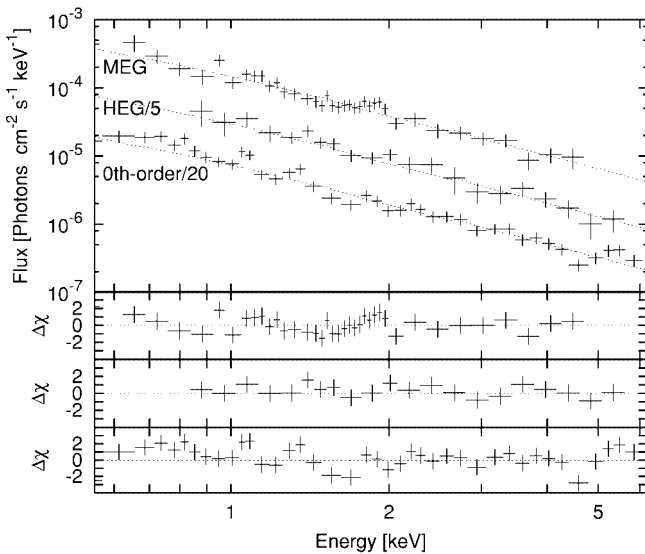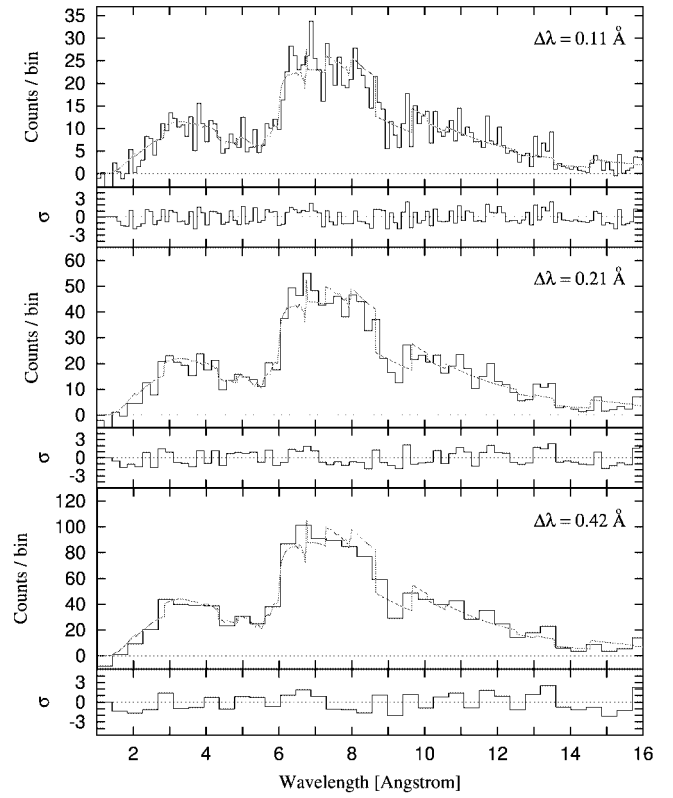

FIG. 7.—The ±1 order HETGS (HEG/MEG) data for GRB 021004 are very well fitted by an absorbed power law (§ 3). The zeroth-order data (S/N ≥ 5 per bin) are also fitted well by this model. Here we divide the HEG data by a factor of 5 and the zeroth-order data by a factor of 20 for ease of viewing.
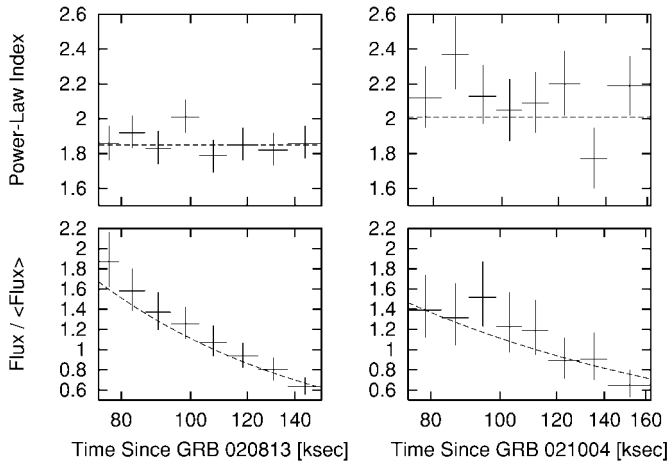
Fig. 9.—To look for spectral variability, the HETGS data for each GRB are divided into eight regions of equal counts and fitted with absorbed power laws by minimizing the Cash statistic (Cash 1979). The above plots show the power-law indexes Γ and the (energy) fluxes found for each fit, with the best-fit values of Γ derived for the entire data set and the best-fit temporal fade found for the count rates overplotted as dashed lines. The fluxes have been divided by the mean fluxes for each observation reported in § 2. Error bars are 90% confidence, determined from the one-parameter confidence intervals.

time. Using the likelihood ratio test, we find evidence for a decrease in equivalent width between the first 28.5 ks of data and the remainder of the observation at 97% confidence ($\Delta\chi^2 = 4.7$ for 1 additional parameter).

5. DISCUSSION

The most significant discrete feature we observe in afterglow spectrum of GRB 020813 is clearly the line we associate with S, which we detect at 3.3 σ significance. This is a somewhat marginal detection. However, the reality of the line is supported by the presence of line counts in various times slices throughout the observation and in each of the four independent first-order spectra (MEG/HEG ± 1 orders). For the full observation no detector anomalies (e.g., flares, flickering pixels) are observed in the ACIS-S CCD regions yielding the HETGS MEG/HEG ± 1 order counts from this line. The background is negligible between 0.6 and 6 keV, contributing only 3% of the total counts. Pileup in the grating spectrum is not a concern for this observation because of the very low count rate. Excess counts corresponding to the line are detected in each independent spectrum, and the numbers are consistent at the 1.5 σ level. The combined first-order spectra (MEG/HEG) show a consistent number of excess counts at the 1 σ level. The validity of this line detection is possibly strengthened by an association with S xvi Kα and by a marginal detection of a line at the expected energy for Si xiv Kα. We have performed a parallel reduction for the GRB 021004 afterglow data, and this has yielded no convincing evidence for discrete spectral features.

Although we find possible evidence for temporal variability in the line emission for GRB 020813 (§ 4), the lines are detected in the full 76.8 ks observation, and the full data set is moderately well fitted by a plasma in collisional ionization equilibrium (§ 3). Figures 4–6 show the line and metallicity parameters that we derive in relation to those reported for

other GRBs in the literature. Our required abundances are only modestly supersolar (§ 3), in contrast to those reported for several other GRBs. The line luminosities are quite low, and the rest-frame equivalent widths are an order of magnitude smaller than those reported for any other GRB. Figure 10 shows the GRB 020813 continuum and S xvi line fluxes versus time alongside the data for GRB 011211 from R02. In comparison to GRB 011211, it appears that the longevity of the line emission (and also the narrowness of the lines) was critical to their detection, whereas the 10 times stronger continuum could easily have hidden less persistent emission.

We can interpret the longer duration and later onset of the lines for GRB 020813 relative to GRB 011211 (Fig. 10) as a purely geometrical effect due to observing emitting material residing at a larger radius R from the GRB. For radially expanding emitting material heated by GRB photons or by the GRB shock, the narrowness of the lines requires that the emission comes from only a small solid angle ($\Omega \lesssim 0.4$), as viewed from the GRB, consistent with GRB beaming models (Frail et al. 2001). The line duration ($t_{\rm line} \gtrsim 76.8$ ks) can be attributed to time delays across a thin shell, and this leads to the requirement $R = (ct_{\rm line}/1 + z) \times (2\pi/\Omega) \gtrsim 10^{16}$ cm. An estimate $R \lesssim 10^{18}$ cm for the maximum likely R is determined using the smallest solid angle found for a GRB jet in Frail et al. (2001). For the reprocessing material to lie this far out from the GRB, it must have gotten there prior to the GRB. The line identifications we have made (§ 3) require a blueshift $\sim 0.1c$, and this high outflow velocity implicates expanding SN ejecta rather than a stellar wind. The SN would have gone off 0.1–10 yr prior to the GRB. The need for a precursor SN can be avoided if the GRB host (absorption) redshift is taken as a lower limit on the redshift, rather than the actual redshift. In that case, an identification of the S xvi and Si xiv lines with Ar xviii and S xvi ($z = 1.53$, no blueshift), respectively, could be made.
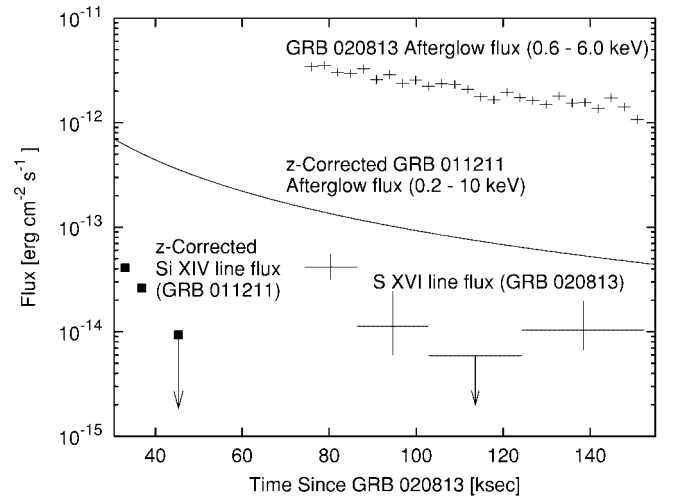

Fig. 10.—Points on the left show the Si xiv Kα line flux for GRB 011211 from R02, corrected to the redshift of GRB 020813. The integrated afterglow flux for GRB 012111 is also plotted and extrapolated. We employ a cosmology with $\Omega_m = 0.3$, $\Omega_\Lambda = 0.7$, and $h = 0.65$. At a later time ($\sim$50 ks later in the GRB frame), we measure a similar line flux. However, the GRB 020813 afterglow flux is approximately an order of magnitude higher that of GRB 011211. On the right, we plot the measured line flux from S xvi Kα, and the afterglow flux, vs. time since GRB 020813. Error bars and the one upper limit are at 1 σ confidence.

BUTLER ET AL.

In the case of GRB 011211, R02 assert that a shell of thermal plasma at $R \sim 10^{15}$ cm can account for the afterglow spectrum and for the duration of the reported emission lines. Taking into account radiation transfer across the shell, Lazzati (2002) argues that a larger radius is required ($R \gtrsim 10^{17}$ cm), because the large afterglow luminosity implies a high density, which implies a cooling time much shorter than the observed line duration. Following Lazzati (2002), we find that a thermal model for GRB 020813 also implies $R \gtrsim 10^{17}$ cm, except for the case (discussed below) where the luminosity of the thermal component is actually overwhelmed by a (~ 10 times brighter) power-law continuum component. In this case, a solution with $R \sim 10^{16}$ cm is possible. The density is low ($n \sim 10^8$ cm^{-3}), and this implies a shell with thickness $dR \sim R/10$ for $\tau_T = 0.1$. At larger radii, the shell must be either very thin or very clumped for the contained mass to be similar to that expected from SNe ($M_{\mathrm{ejecta}} \lesssim 20\ M_\odot$; Woosely & Weaver 1995).

We see three reasons, which arise from complexities in our modeling, to be cautious in interpreting our results as evidence for a persistent thermal component. First, we observe lines with best-fit widths an order of magnitude larger than the thermal line widths. We account for this in the thermal model by introducing a turbulence velocity of 2000 km s^{-1}. It is also possible that this broadening is kinematical. Second, the best-fit CIE plasma model has marginally dissimilar abundances for the multiple-α elements (Fig. 4) and very low abundances for the Fe group elements relative to the multiple-α elements (Fig. 4 and Fig. 3, inset). This would require an unusual chemical composition for the emitting medium, a mechanism beyond the APED model for suppressing emission from metals other than Si and S, or the addition of a power-law continuum component to the model as discussed in § 3. Third, the data do not tightly constrain the relative contributions to the continuum from the CIE plasma and from this possible power-law component. Indeed, the continuum appears nonthermal, as would be expected for the X-ray afterglow of the burst.

Although these considerations do not rule out a thermal model, reflection models may more naturally describe a spectrum with broad lines superposed on a power-law continuum (see, e.g., Ballantyne et al. 2001; Vietri et al. 2001). In these models, the line broadening is due to Compton scattering. If the electron temperature is similar to the line energy, we expect $\sigma_E/E \sim (kT/m_e c^2)^{1/2} \sim 0.05$ (at 1.3 keV) for a single scattering. Because this is already a factor ~ 5 times larger than the observed widths, we require the reflector to not be highly ionized. Consulting Figure 2 of Lazzati, Ramirez-Ruiz, & Rees (2002), it appears that our observed dissimilarity in line luminosities (Table 1, Fig. 5) may further reinforce this conclusion. Their reflection models with ionization parameter ξ in the range $10 < \xi < 100$ can produce Si and S line luminosities that are an order of magnitude greater than luminosities of lines from Ar, Ca, and Fe. In the case of GRB 011211, Lazzati et al. (2002) argue that the large line equivalent widths rule out nearby reprocessor models. This is not the case for GRB 020813, and the line duration may be set by a delayed energy injection rather than by the geometry of the reprocessing material (see Rees & Mészáros 2000; Mészáros & Rees 2001). In this case, we would not need a two-step (SN then GRB) explosion.

In conclusion, we detect lines from an overabundance of light metals characteristically produced in massive stars during presupernova nucleosynthesis in the X-ray afterglow of GRB 020813. The long S xvi line duration and narrow line widths can be explained via the geometry of the emitting material, and this would likely require a two-step explosion as in the supranova (Vietri & Stella 1998) scenario. The time delay between the SN and GRB is $\gtrsim 2$ months in this picture. In contrast, our weak detection of a Ni feature, with no detection of Fe (or Co), suggests a very short time delay ($\lesssim 1$ week) between the SN and the GRB. As discussed in Woosely, Zhang, & Heger (2002), it is not likely possible to observe a GRB through a supernova remnant this young; the Ni feature may indicate that the geometric picture is wrong. A thermal model adequately fits the full data set. A bright Fe (or Ni or Co) feature is not observed, however, and this is perhaps the strongest reason to favor a reflection model, where an Fe line can be quenched by Auger autoionization (Lazzati et al. 2002).

REFERENCES

Antonelli, L. A., et al. 2000, ApJ, 545, L39
Ballantyne, D. R., et al. 2001, ApJ, 559, L83
Bloom, J. S., et al. 1999, Nature, 401, 453
Borozdin, K. N., & Trudoyubov, S. P. 2003, ApJ, 583, L57
Cash, W. 1979, ApJ, 228, 939
Fox, D. W. 2002, GCN Circ. 1564
Fox, D. W., & Blake, C. 2002, GCN Circ. 1470
Frail, D. A., et al. 2001, ApJ, 562, L55
Galama, T., et al. 1998, Nature, 395, 670
Halpern, J., et al. 2002, GCN Circ. 1578
Holland, S. T., et al. 2003, AJ, 125, 2291
Jansen, F., et al. 2001, A&A, 365, L1
Kouveliotou, C., et al. 1993, ApJ, 413, L101
Kulkarni, S. R., et al. 1998, Nature, 395, 663
———. 1999, Nature, 398, 389
Lazzati, D. 2002, A&A, 399, 913
Lazzati, D., Ramirez-Ruiz E., & Rees, M. J. 2002, ApJ, 572, L57
Malesani, D., et al. 2002, GCN Circ. 1500
Marshall, H. L., et al. 2002, ApJ, 564, 941
Mészáros, P., & Rees, M. 2001, ApJ, 556, L37
Mirabel, N., et al. 2002, GCN Circ. 1618
Piro, L., et al. 1999, A&AS, 138, 431
———. 2000, Science, 290, 955
Price, P. A., et al. 2002, GCN Circ. 1475
Protassov, R., et al. 2002, ApJ, 571, 545

Rauscher, T., et al. 2002, ApJ, 576, 323
Rees, M., & Mészáros, P. 2000, ApJ, 545, L73
Reeves, J. N., Watson, D., Osborne, J. P., Pounds, K. A., & O'Brien, P. T. 2003, MNRAS, 403, 463
Reeves, J. N., et al. 2002, Nature, 415, 512 (R02)
Reichart, D. E. 2001, ApJ, 554, 643
Ricker, G. R., et al. 2003, in AIP Conf. Proc. 662, Gamma-Ray Burst and Afterglow Astronomy 2001, ed. G. Ricker & R. Vanderspek (New York: AIP), 3
Rutledge, S., & Sako, M. 2002, MNRAS, 339, 600
Sahu, K. C., et al. 1997, Nature, 387, 476
Sako, M., & Harrison, F. A. 2002, GCN Circ. 1624
Shirasaki, Y., et al. 2002, GCN Circ. 1565
Vanderspek, R., et al. 2002, GCN Circ. 1504
Vietri, M., & Stella, L. 1998, ApJ, 507, L45
Vietri, M., et al. 2001, ApJ, 550, L43
Villasenor, J., et al. 2002, GCN Circ. 1471
Watson, D., et al. 2002, A&A, 393, L1
Weisskopf, M. C., et al. 2002, PASP, 114, 1
Woosely, S. E., & Weaver, T. A. 1995, ApJS, 101, 181
Woosely, S. E., Zhang, W., & Heger, A. 2003, in AIP Conf. Proc. 662, Gamma-Ray Burst and Afterglow Astronomy 2001, ed. G. Ricker & R. Vanderspek (New York: AIP), 185
Yoshida, A., et al. 1999, A&AS, 138, 433